Plasmon resonance coupling in strongly coupled gold nanotube arrays with structural defects*

Zhou Xin(周 昕)†, Fang Jian-Shu(方见树), Yang Di-Wu(杨迪武), and Liao Xiang-Ping(廖湘萍)

School of Sciences, Hunan University of Technology, Zhuzhou 412008, *China*

(Received 11 January 2012; revised manuscript received 17 February 2012)

We theoretically investigate the transmission spectra and the field distributions with different defects in the gold nanotube arrays by using the finite-difference time-domain method. It is found that the optical properties of the nanotube arrays are strongly influenced by different defects. When there are no defects in the central nanotube, the values of peaks located at both sides of the photonic band gap have their maxima. Based on the distributions of electric field component E_x and the total energy distribution of the electric and the magnetic field, we show that mainly a dipole field distribution is exhibited for the plasmon mode at the long-wavelength edge of the band gap but higher order modes of the composite are excited at the short-wavelength edge of the band gap. The plasmon resonant modes can also be controlled by introducing defects.

Keywords: structural defect, transmission spectra, gold nanotube array, field distributions

PACS: 42.25.Bs, 73.20.Mf, 73.63.–b **DOI:** 10.1088/1674-1056/21/8/084202

1. Introduction

The electronic and optical properties of metallic nanostructures are important from both a technological and a scientific perspective.[1,2] The resonant oscillations of free electrons in metallic materials, termed surface plasmon resonances (SPR), have properties determined by the structure of the metal, and can ultimately be tailored to impart new optically-induced functionalities into materials for specific practical uses. In addition, the plasmon resonance can lead to large enhancements in the local electric fields close to the metal surface. Enhanced electromagnetic (EM) field effects can be generated either in a broad spectral range, as is the case for disordered metal-dielectric composites,[3,4] or at selected frequencies from periodically ordered metal nanostructures. Ordered arrays of metal nanoparticles are of interest for the development of optical waveguides,[5,6] optical circuits, surface-enhanced Raman scattering (SERS),[7,8] subdiffractional microscopy, and bio-chemical sensors.[9−11] Collective SPR modes, which stem from the electromagnetic coupling between nanoparticles, make it possible to transfer optical signals along the nanoparticle array and use them as transducers of molecular vibrational signatures into optical spectra.[12−14]

Metallic nanotubes, which can be made by forming air holes inside the metallic nanocylinder (the core-shell nanocylinder), have also attracted great attention for the possibility of their use as interconnects in very large scale integrated circuits[15] and field emission devices.[16] For this nanostructure the tunable resonances arise from the interaction and mixing of two fixed-frequency plasmons, and those of a wire (the outer surface of the metallic tube) and a capillary (the inner surface of the tube). This interaction results in a splitting of the plasmon resonances into a lower energy (symmetric) plasmon and a higher energy (antisymmetric) plasmon.[17] The energies of these two eigenmodes are determined by the strength of the interaction between the wire and capillary plasmons, which is controlled by the thickness of the tube. A thin tube results in strong plasmon mixing and the larger splitting of the plasmons, while a thick tube effectively isolates the plasmons of the two surfaces.

In this paper, we explore how the plasmonic behaviours of the coupled gold nanotube (core-shell nanocylinder) arrays depend on different defects.

*Project supported by the Scientific Research Foundation of Hunan Provincial Education Department, China (Grant Nos. 11C0425 and 09C314), the Natural Science Foundation of Hunan Province, China (Grant No. 10JJ3088), the Major Program for the Research Foundation of Education Bureau of Hunan Province, China (Grant No. 10A026), and the National Natural Science Foundation of China (Grant No. 11164007).

†Corresponding author. E-mail: xzhou522@ yahoo.com.cn

© 2012 Chinese Physical Society and IOP Publishing Ltd

When the point defects are introduced, the input beam is modulated by different defects. So the defects can significantly affect the energies of plasmon resonances of the gold nanotube arrays. We calculate the transmission spectra and the electric field distributions of this structure, and show that the plasmon resonances strongly depend on the defects.

2. Model and theory

As an effective numerical algorithm for the exact solution to Maxwell's equations, the finite-difference time-domain (FDTD) method and its ramification are a highly useful tool in studying the electromagnetic responses and optical properties of nanostructures.[18−21] In our work, we simulate the transmission spectra and the distributions of the field intensity of nine gold nanotubes arrays, as depicted schematically in Fig. 1, by the FDTD method. The hollow gold nanotube arrays are placed in air. The outer radius, inner radius, and the separation distance are set respectively to be $R_1 = 50$ nm, $R_2 = 40$ nm, and $d = 120$ nm when the nanotube arrays have no defects. We simulate the structure with an FDTD cube of size $L_x \times L_y = 1600$ nm $\times$ 200 nm and infinity along the z direction. The spatial and temporal steps are set at $\Delta x = \Delta y = 1$ nm, and $\Delta t = \Delta x/2c$ (c is the velocity of light in a vacuum). Instead of studying the steady-state response, one frequency at a time, we send a Gaussian single pulse of light with a wide frequency profile. The incident light polarizes along the y axis and irradiates the structure along the x direction in our work. Perfectly matched absorbing boundary conditions are applied at the left and right surfaces of the computational space along the x direction, whereas periodic boundary conditions are applied to other boundaries along the y direction.

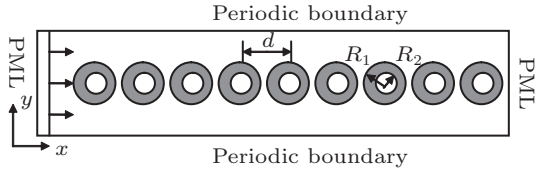


Fig. 1. Top view of a single infinitely long gold nanotube array (outer radius R_1, inner radius R_2) with 9 nanotubes. The interparticle spacing between adjacent nanotubes is denoted with d. Periodic boundary conditions are imposed on the surfaces along the y direction, while perfect matched layers (PML) are imposed on the surfaces along the x direction.

The nanotube thickness here is 10 nm, less than the gold electron mean-free path ($\sim$ 42 nm). When the thickness of the tube becomes smaller than the mean free path of conduction electrons in bulk metal, one should take into account the size effect caused by the scattering of the conduction electrons from the walls of the particle and interface tunneling into adsorbate states.[22,23] This effect can be taken into account by modifying the dielectric function of the Au nanotube using the Drude model for the conduction electrons:[22]

$$\varepsilon(\omega) = \varepsilon_\infty - \frac{\omega_{\rm p}^2}{\omega^2 + {\rm i}\omega\gamma_{\rm p}}, \tag{1}$$

where $\omega_{\rm p} = 1.37 \times 10^{16}$ s^{-1} is the bulk plasmon frequency of the gold, ω is the angle frequency of the incident wave, $\varepsilon_\infty = 1$ is the instantaneous relative dielectric constant at the infinite-frequency, and $\gamma_{\rm p} = 4.08 \times 10^{13}$ s^{-1} represents the damping rate which characterizes the Ohmic absorption loss. These values are obtained by fitting the experimental results.[24]

3. Results and discussion

For comparison, in Fig. 2, we first investigate the transmission spectrum of the gold nanotube array as a function of wavelength without defects. The figure clearly shows that there exists one large photonic band gap (PBG) at wavelengths from 0.4137 μm to 0.5905 μm. At wavelengths within the bandgap, the density of SP modes is zero, thus no SP modes can be supported. The resonant peaks that are located at the short-wavelength edge of the bandgap are dense and irregular, whereas the resonant peaks at the long-wavelength edge of the bandgap are regular. Meanwhile, in the long-wavelength region, the transmission becomes higher with wavelength increasing.

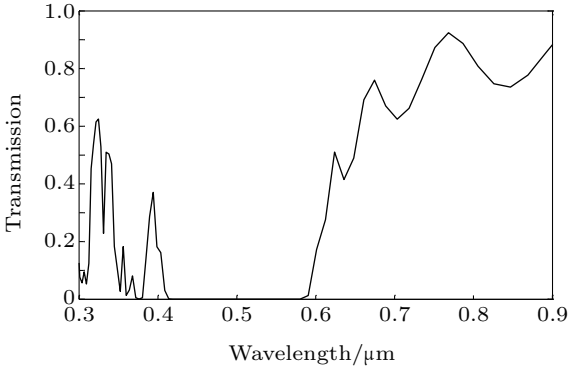


Fig. 2. Transmission spectrum as a function of wavelength for the hollow metallic nanotube array with $R_1 = 50$ nm, $R_2 = 40$ nm, and $d = 120$ nm.

The transmission spectra of the nanotube arrays each as a function of wavelength with defects, obtained

by removing a specified nanotube: (a) the second nanotube, (b) the third nanotube, (c) the fourth nanotube, (d) the central nanotube, are shown in Fig. 3. It can be seen clearly that the resonant peaks close to the short-wavelength edge of the PBG and the peaks located at 0.674 μm are weakened remarkably. For example, compared with Fig. 2, the transmission of the peak located at 0.394 μm is weakened from 0.3707 to 0.0934 and the peak located at 0.674 μm vanishes in Fig. 3(c). This phenomenon can be explained by two points. Firstly, the action of removing a specified particle results in the intertube distance becoming farther apart. So the electromagnetic interactions between them do not play a significant role, and almost only excitation of localized plasmon takes place. However, the interference effect between the nanotubes is still present. Secondly, the larger distance of the defects from the nanotube arrays' interface reduces their coupling to the incident beam and leads to a smaller even absent resonance amplitude.[25]

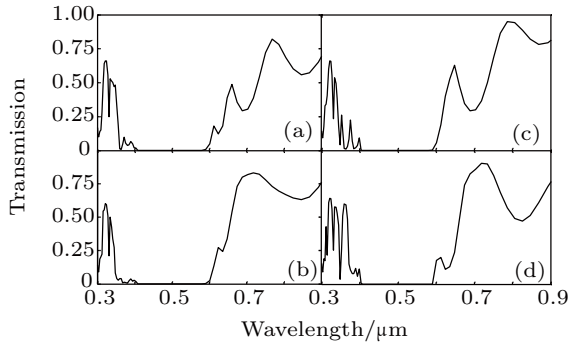


Fig. 3. Transmission spectra of the nanotube arrays with defects by removing the second nanotube (a), the third nanotube (b), the fourth nanotube (c), and the central nanotube (d).

In Fig. 4, we show the transmission spectra of the gold nanotube arrays each as a function of wavelength with defects, obtained by changing the core dielectric constant ε of the central nanotube of (a) $\varepsilon = 2$, (b) $\varepsilon = 3$, and (c) $\varepsilon = 4$. Taking one with another, compared with the scenario in Fig. 2, this defect results in the lower values of the resonant peaks which are close to two sides of the PBG, slight blue-shifts of the peaks which are close to the long-wavelength edge of the PBG and the enhancements of the peaks which are located at the maximal long-wavelength position. The peak close to the long-wavelength edge of the PBG shifts from 0.6238 μm to 0.6012 μm, when we introduce the defect. It also consequently induces the narrower bandgap. On the other hand, the decreased resonant peaks are gradually enhanced with the increase of the core dielectric constant of the central nanotube ε. The resonance peaks shown with the arrows pointing down augment from 0.0423 to 0.2019 and the peaks located at 0.6012-μm augment from 0.0349 to 0.1942 when ε increases from 2 to 4. When the nanotube is placed in a time-dependent external field, the dielectrics will polarize and produce an additional component to the excitation field across the nanotube. The electrons will screen not only the original excitation field, but also the field produced by the dielectric.[26]

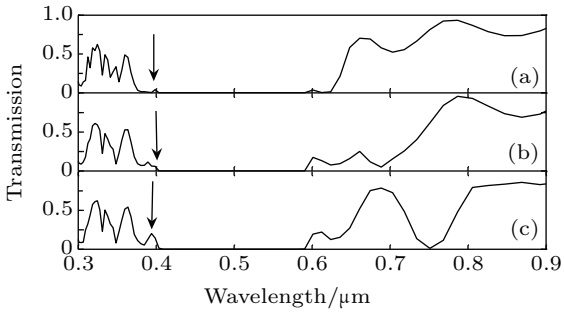


Fig. 4. Transmission spectra each as a function of wavelength for the metallic nanotube arrays with core dielectric constant of the central nanotube $\varepsilon = 2$ (a), 3 (b), and 4 (c).

Fundamental modes of nanotube plasmons can also be illustrated with electric field distributions on the nanostructures. To reveal the physical mechanism behind the resonance peaks, we discuss the spatial distributions of the electric field. Different modes mean many different couplings of plasmons, and we can know more information about the resonance modes by describing the distribution of the electric field. Figure 5 shows the instantaneous electric field component E_x (panels (a)–(c)) and the total energy distribution of the electric and the magnetic field (panels (d)–(f)) at the peaks close to the longer wavelength photonic band edge in Fig. 4 for different values of ε. The three resonance peaks in Figs. 4(a)–4(c) are all located at 0.6012 μm. We can see that the distributions of the electric field component E_x are regular. Positive and negative fields alternately appear in the gap of the nanotubes and mainly the dipole field distribution for the plasmon mode in the nanotube arrays. The existence of a dielectric gap means that the intertube interaction is highly capacitive in nature, and therefore a number of opposing surface charges builds up on the tubes. The existence of a dielectric gap means that the intertube interaction is highly capacitive in nature, and therefore a number of opposing surface charges build up in the gap between adjacent nanotubes. When the signs of the surface charges at the

two sides of the gap are opposite, the electric fields in the gap are coupled together closely and intensified, which is just in analogy to a simple capacity device. On the contrary, when they are uniform and repulsive to each other, the electric fields are decoupled and become very weak. It is also found that the outside electrical field is only located within a few nanometers of the tube surface and there is no E_x distribution inside the nanotubes. With the increase of the core dielectric constant ε of the central nanotube, E_x distribution at the central nanotube becomes discontinuous, whereas E_x distribution at the last nanotube is strengthened. One of the reasons for the discontinuity of the electric field at the central nanotube may be attributed to the increase of ε of the central nanotube, resulting in increased absorption efficiency and less interaction between the incident light and the nanotubes. Panels (d)–(f) in Fig. 5 clearly show that the total energy is mostly concentrated in the front of the nanotube arrays. However, the total energy is strengthened gradually at the tail of the nanotube arrays with the increase of ε.

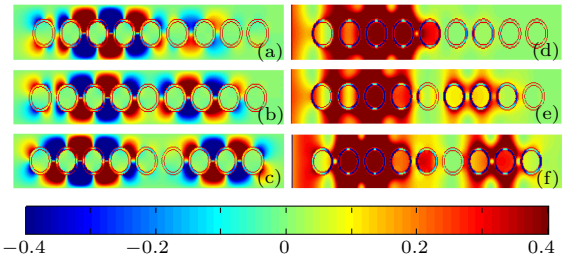


Fig. 5. (colour online) Instantaneous electric field distributions at three different resonance peaks that are shown in Figs. 4(a)–4(c), the resonance peaks are 0.6012 μm, 0.6012 μm, and 0.6012 μm, respectively. Panels (a)–(c) show the instantaneous electric field component E_x distributions and the panels (d)–(f) the total energy distributions of magnetic and electric fields.

Figures 6(a)–6(c) show the spatial images of the instantaneous electric field component E_x at a steady state for the different resonance peaks shown with the arrows pointing down in Fig. 4. For the multitube system, interactions between nanotubes allow a greater degree of freedom for plasmon resonances to occur. Furthermore, it is well known that plasmonic nanoparticles may support higher-order localized resonances at optical frequencies, even when their total size is much smaller than the wavelength. Compared with dipole field distributions in Figs. 5(a)–5(c), we can see that composite higher order plasmon modes appear in the array of the nanotubes, one for each in Figs. 6(a)–6(c). In physical terms, the multipolar nature of nanotube plasmons is closely related to spherical harmonics, in which the expansion orders directly correspond to dipoles, quadrupoles, octopoles, and so forth. Besides, note that each nanotube should remain electrically neutral, for the surface charges are all induced by polarizations.

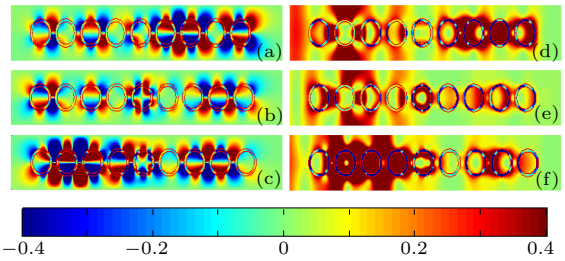


Fig. 6. (colour online) The instantaneous electric field distributions at three different resonance peaks shown with the arrows pointing down in Figs. 4(a)–4(c), where the resonance peaks are located at 0.3988 μm, 0.3894 μm, and 0.3941 μm, respectively. Panels (a)–(c) show the instantaneous electric field component E_x distributions and the panels (d)–(f) the total energy distribution of magnetic and electric fields.

The total energy distributions of the electric and the magnetic fields at the peaks shown with the arrows pointing down in Fig. 4 are obtained as shown in Figs. 6(d)–6(f). The total energy distributing around the central nanotube slightly strengthens with the increase of ε. The total energy mainly concentrates around the tail of the nanotube arrays when $\varepsilon = 2$, whereas it mainly concentrates around the front of the nanotube arrays as $\varepsilon = 4$.

In this section, we discuss the effect of the radius of the central nanotube on the transmission spectrum of the nanotube arrays. Figure 7 shows the transmission spectra of gold nanotube arrays when the radii of the central nanotube are (a) $R_{15} = 60$ nm, $R_{25} = 50$ nm, (b) $R_{15} = 65$ nm, $R_{25} = 55$ nm, (c) $R_{15} = 35$ nm, $R_{25} = 25$ nm, (d) $R_{15} = 40$ nm, $R_{25} = 30$ nm, respectively. The outer radius and inner radius of the central nanotube are denoted with R_{15} and R_{25}. The resonant peaks at the two sides of the PBG are weakened, and the number of peaks in the short-wavelength region decreases as the radius increases. When the radius decreases, compared with the scenario in Fig. 2, the peaks in the short-wavelength region are all weakened, the peak located at 0.6238 μm is blue-shifted to 0.6123 μm and weakened, but the peak located at 0.6746 μm is enhanced. To conclude, the resonant states located at both sides of the PBG are primarily rooted from the interaction

between the central nanotube and the adjacent nanotubes. When there are no defects in the central nanotube, the values of the peaks located at both sides of the PBG have their maxima.

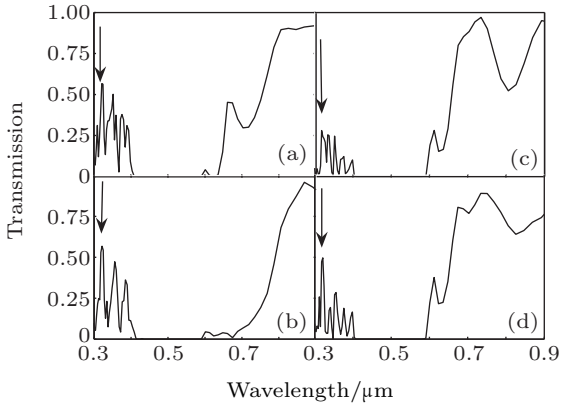


Fig. 7. Transmission spectra each as a function of wavelength for gold nanotube arrays with outer (R_{15}) and inner (R_2) radius of the central nanotube R_{15} = 60 nm, R_{25} = 50 nm (a), R_{15} = 65 nm, R_{25} = 55 nm (b), R_{15} = 35 nm, R_{25} = 25 nm (c), and R_{15} = 40 nm, R_{25} = 30 nm (d).

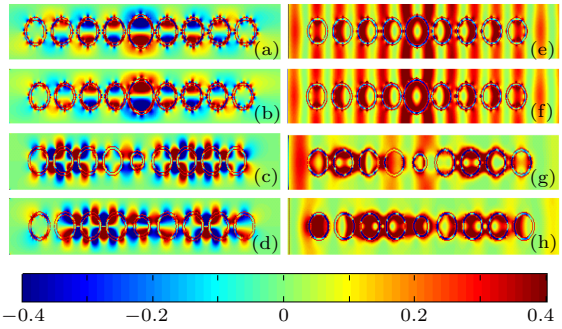


Fig. 8. (colour online) Instantaneous electric field distributions at three different resonance peaks shown with the arrows pointing down in Figs. 7(a)–7(d). Panels (a)–(d) show the instantaneous electric field component E_x distributions and the panels (e)–(h) the total energy distribution of magnetic and electric fields.

In Fig. 8, we show and compare the spatial distributions of the instantaneous electric field component E_x (panels (a)–(d)) and the total energy distribution of the electric and the magnetic field (panels (e)–(h)) at a steady state for the resonance modes shown with arrow pointing down in Figs. 7(a)–7(d). We can see that these resonant peaks exhibit composite higher order modes. Figures 5, 6, and 8 show that the peaks located at a shorter wavelength have higher-order plasmon modes in the system under study. The dipoles field distribution only exists outside the nanotube, but the higher-order plasmon modes appear not only outside the nanotube but also inside the nanotube. Interestingly, when the radius of the central nanotube increases, the total energy mainly occurs along the polarization direction (y direction) in Figs. 8(e) and 8(f). This phenomenon is especially distinct around the central nanotube. In contrast, the total energy occurs along the spread direction (x direction) and is mostly concentrated inside the nanotubes (Figs. 8(g) and 8(h)) as the radius of the central nanotube decreases.

4. Conclusions

In this paper, we theoretically investigated the transmission spectra and the field distributions with different defects in the gold nanotube arrays, using the FDTD method. Firstly, we showed the case where there are no defects in the gold nanotube arrays. Then, we removed a specific nanotube, and changed the radius and the core dielectric constant of the central nanotube. We found that the resonant states located at both sides of the PBG are rooted primarily from the interaction between the central tube and the adjacent tubes. When there are no defects in the central nanotube, the values of the peaks located at both sides of the PBG have their maxima. According to the field distributions, we showed that mainly a dipole field distribution is exhibited for the plasmon mode at the long-wavelength edge of the band gap but composite higher order modes are excited at the short-wavelength edge of the band gap. We also showed that the peaks located at shorter wavelength have higher-order plasmon modes in the system under study. The plasmon resonant modes can be controlled by introducing defects. These results obtained here may provide potential applications in novel plasmonic devices.

References

[1] Cheng M T 2011 *Acta Phys. Sin.* **60** 117301 (in Chinese)
[2] Maier S A, Brongersma M L, Kik P G, Meltzer S, Requicha A A G and Atwater H A 2001 *Adv. Mater.* **13** 1501
[3] Shen Y, Fan D H, Fu J W and Yu G P 2011 *Acta Phys. Sin.* **60** 117302 (in Chinese)
[4] Sarychev A K and Shalaev V M 2000 *Phys. Rep.* **335** 275
[5] Hicks E M, Zou S, Schatz G C, Spear K G, Duyne P V, Gunnarsson L, Rindzevicius T, Kasemo B and Kaell M 2005 *Nano Lett.* **5** 1065
[6] Wei Q H, Su K H, Durant S and Zhang X 2004 *Nano Lett.* **4** 1067
[7] Félidj N, Aubard J, Lévi G, Krenn J R, Salerno M, Schider G, Lamprecht B, Leitner A and Aussenegg F R 2002 *Phys. Rev.* B **65** 075419

[8] Félidj N, Aubard J, Lévi G, Krenn J R, Hohenau A, Schider G, Leitner A and Aussenegg F R 2003 *Appl. Phys. Lett.* **82** 3095

[9] Haynes C L, McFarland A D, Zhao L L, Van Duyne R P, SchatzG C, Gunnarsson L, Prikulis J, Kasemo B and Kall M 2003 *J. Phys. Chem.* B **107** 7337

[10] Haes A J, Zou S L, Schatz G C and Van Duyne R P 2004 *J. Phys. Chem.* B **108** 109

[11] Hao E, Li S Y, Bailey R C, Zou S L, Schatz G C and Hupp J T 2004 *J. Phys. Chem.* B **108** 1224

[12] Yonzon C R, Jeoung E, Zou S, Schatz G C, Mrksich M and Van Duyne R P 2004 *J. Am. Chem. Soc.* **126** 12669

[13] Hao E C, Kelly K L, Hupp J T and Schatz G C 2002 *J. Am. Chem. Soc.* **124** 15182

[14] Xie S X, Li H J, Xu H Q, Zhou X and Fu S L 2010 *Chin. Phys.* B **19** 077803

[15] Kreup F, Graham A P, Liebau M, Duesberg G S, Seidel R and Unger E 2004 *Tech. Dig. Int. Electron Dev. Meeting* 683

[16] Patil A, Ohashi T, Buldum A and Dai L 2006 *Appl. Phys. Lett.* 89 103103

[17] Moradi A 2008 *J. Phys. Chem. Solids* **69** 2936

[18] Dmitriev A, Pakizeh T, Käll M and Sutherland D S 2007 *Small* **3** 294

[19] Oubre C and Nordlander P 2004 *J. Phys. Chem.* B **108** 17740

[20] Foteinopulou S, Vigneron J P and Vandenbem C 2007 *Opt. Express* **15** 4253

[21] Zhou X, Li H J, Xie S X, Fu S L, Xu H Q and Wu J J 2010 *Chin. Phys.* B **19** 127806

[22] Kreibig U and Vollmer M 1995 *Optical Properties of Metal Clusters, Springer Ser. Mater. Sci. 25* (Springer: Berlin)

[23] Pinchuk A and Kreibig U 2003 *New J. Phys.* **5** 151

[24] Palik E D 1991 *Handbook of Optical Constants in Solids* (Boston: Academic) Vol. 1

[25] Gadot F, de Lustrac A, Lourtioz J M, Brillat T, Ammouche A and Akmansoy E 1999 *J. Appl. Phys.* **85** 8499

[26] Prodan E, Lee A and Nordlander P 2002 *Chem. Phys. Lett.* **360** 325